

MIT Open Access Articles

Nonlinear microscopy for detection of prostate cancer: analysis of sensitivity and specificity in radical prostatectomies

The MIT Faculty has made this article openly available. **Please share** how this access benefits you. Your story matters.

Citation: Cahill, Lucas C. et al. "Nonlinear microscopy for detection of prostate cancer: analysis of sensitivity and specificity in radical prostatectomies." 33, 5 (November 2019): 916–923 © 2019 The Author(s)

As Published: <http://dx.doi.org/10.1038/s41379-019-0408-4>

Publisher: Springer Science and Business Media LLC

Persistent URL: <https://hdl.handle.net/1721.1/128835>

Version: Author's final manuscript: final author's manuscript post peer review, without publisher's formatting or copy editing

Terms of Use: Article is made available in accordance with the publisher's policy and may be subject to US copyright law. Please refer to the publisher's site for terms of use.





Published in final edited form as:

Mod Pathol. 2020 May ; 33(5): 916–923. doi:10.1038/s41379-019-0408-4.

Nonlinear microscopy for detection of prostate cancer: analysis of sensitivity and specificity in radical prostatectomies

Lucas C. Cahill^{1,2}, Yubo Wu³, Tadayuki Yoshitake², Cecilia Ponchiardi³, Michael G. Giacomelli², Andrew A. Wagner⁴, Seymour Rosen^{3,*}, James G. Fujimoto^{2,*}

¹Harvard-MIT Division of Health Sciences and Technology, Harvard Medical School and Massachusetts Institute of Technology, Cambridge, MA, USA

²Department of Electrical Engineering and Computer Science and Research Laboratory of Electronics, Massachusetts Institute of Technology, Cambridge, MA, USA

³Department of Pathology, Beth Israel Deaconess Medical Center, Harvard Medical School, Boston, MA, USA

⁴Department of Surgery, Division of Urology, Beth Israel Deaconess Medical Center, Harvard Medical School, Boston, MA, USA

Abstract

Intraoperative evaluation of specimens during radical prostatectomy using frozen sections can be time and labor intensive. Nonlinear microscopy (NLM) is a fluorescence microscopy technique that can rapidly generate images that closely resemble H&E histology in freshly excised tissue, without requiring freezing or microtome sectioning. Specimens are stained with nuclear and cytoplasmic/stromal fluorophores, and nonlinear microscopy evaluation can begin within 3 minutes of grossing. Fluorescence signals can be displayed using an H&E color scale, facilitating pathologist interpretation. This study evaluates the accuracy of prostate cancer detection in blinded reading of nonlinear microscopy images compared to the gold-standard of formalin fixed, paraffin embedded H&E histology.

A total of 122 freshly excised prostate specimens were obtained from 40 patients undergoing radical prostatectomy. The prostates were grossed, dissected into specimens of ~10×10 mm with 1–4 mm thickness, stained for 2 minutes for nuclear and cytoplasmic/stromal contrast, and then rinsed with saline for 30 seconds. Nonlinear microscopy images were acquired and multiple images were stitched together to generate large field of view, centimeter-scale digital images suitable for reading. Specimens were then processed for standard paraffin H&E. The study protocol consisted of training, pre-testing, and blinded reading phases. After a washout period, pathologists read corresponding paraffin H&E slides.

Users may view, print, copy, and download text and data-mine the content in such documents, for the purposes of academic research, subject always to the full Conditions of use:http://www.nature.com/authors/editorial_policies/license.html#terms

Correspondence sent to: James G. Fujimoto, Massachusetts Institute of Technology, 50 Vassar St, Bldg 36-345, Cambridge, MA 02139, Phone: 617-253-8528, Fax: 617-253-9611, jgfuj@mit.edu.
*co-senior author

Disclosure/Conflict of Interest

JGF, MGG, TY, and LCC are inventors on patent application WO2017139649: Method and apparatus for imaging unsectioned tissue specimens. All other authors have no conflicts of interest to declare.

Three pathologists achieved a 95% or greater sensitivity with 100% specificity for detecting cancer on nonlinear microscopy compared to paraffin H&E. Pooled sensitivity and specificity was 97.3% (93.7%–99.1%; 95% confidence interval) and 100.0% (97%–100%), respectively. Interobserver agreement for nonlinear microscopy reading had a Fleiss $\kappa=0.95$. The high cancer detection accuracy and rapid specimen preparation suggest that nonlinear microscopy may be useful for intraoperative evaluation in radical prostatectomy.

Prostate cancer is the highest incidence malignancy in the U.S. male population, with an estimated 160,000 new cases and 29,000 deaths attributed to the disease in 2018.¹ Treating localized prostate cancer with radical prostatectomy provides good oncological outcomes and long-term survival benefits.^{2,3} Nerve-sparing radical prostatectomies are favored if cancer does not involve the neurovascular bundles as patients have better recovery of sexual function and urinary continence.^{4–13} However, identifying patients eligible for nerve-sparing can be challenging using existing preoperative staging methods, leading to a higher rate of non-nerve sparing radical prostatectomies than necessary.^{14–17} Comprehensive intraoperative evaluation of prostate surgical margins using frozen sections has been shown to increase rates of nerve-sparing radical prostatectomies, while decreasing positive surgical margin rates.^{18,19} However, comprehensive frozen section assessment of margins is time and labor intensive, which is impractical and expensive for many hospitals.^{18,20} Techniques that can rapidly evaluate fresh surgical specimens without freezing and microtome sectioning are therefore needed.

Nonlinear microscopy (NLM) is a fluorescence microscopy technique that can generate subcellular resolution images that closely resemble H&E stained sections of formalin-fixed, paraffin embedded tissue (subsequently referred to as ‘paraffin H&E’), however imaging can be performed in freshly excised tissue without freezing or microtome sectioning. Nonlinear microscopy generates images by scanning a focused short pulse laser beam on the specimen, which nonlinearly excites fluorescence only at the laser focus, producing an optical sectioning effect over a limited depth range comparable to the thickness of a frozen section.²¹ The fluorescence signals are detected and displayed as a function of the focused laser position in order to generate a digital image. Prostate specimen imaging has also been investigated using other optical techniques such as structured illumination microscopy^{22,23}, microscopy with UV surface excitation²⁴, light sheet microscopy²⁵, and confocal microscopy²⁶. Initial results using these methods have been promising, however studies have largely focused on feasibility and larger scale validation of tissue handling methods, imaging, and quantitative diagnostic accuracy are necessary. Compared with other methods nonlinear microscopy has the advantage that it can image without physical sectioning, so images are acquired rapidly without loss or destruction of tissue. Nonlinear microscopy can image at depths of up to 100 μm ^{27–30}, avoiding surgical debris, surface artifacts, or areas of electrocautery.³¹ This capability is analogous to serial sectioning in histology, except that image depth can be continuously and rapidly adjusted, providing the pathologist with additional information beyond frozen sections. Nonlinear microscopy achieves superior contrast and image quality compared with other imaging modalities^{25,29–31}, making it particularly well-suited for visualizing nuclear and cytoplasmic/stromal detail.

We have previously demonstrated a rapid tissue preparation and imaging protocol where freshly excised prostate tissue is stained in a nuclear and cytoplasmic/stromal fluorescent dye then evaluated using nonlinear microscopy.^{27,32} This protocol generated images which closely resembled those of corresponding paraffin H&E.³² Pathologists were able to visualize prostate tissue architecture, secretory and basal cells, inflammation, and stromal and glandular hyperplasia. We also showed that nonlinear microscopy enabled visualization of prostate carcinoma including Gleason patterns, perineural invasion, extraprostatic extension, and positive margins. This previous study provided a qualitative, descriptive analysis of fresh prostate tissue visualized using nonlinear microscopy compared to paraffin H&E, an important first step in interpreting nonlinear microscopy images, but did not quantitatively assess the diagnostic capability of nonlinear microscopy image interpretation. In this manuscript, we report a multi-pathologist blinded reading study of nonlinear microscopy images from 122 freshly excised prostate tissue specimens from 40 patients to assess the accuracy of nonlinear microscopy for detecting carcinoma.

MATERIALS AND METHODS

Specimen Preparation and Imaging

Freshly excised prostate tissue was collected from patients who underwent a radical prostatectomy using protocols approved by Beth Israel Deaconess Medical Center Committee on Clinical Investigations and Institutional Review Board and Massachusetts Institute of Technology Committee on the Use of Humans as Experimental Subjects. Informed consent was waived by both committees.

The freshly excised prostate tissue was prepared using protocols previously described and shown in Fig. 1A.^{28,32} The fresh prostates were grossed following standard protocols then dissected into specimens of ~10×10 mm with 1–4 mm thickness. The unprocessed specimens were stained in a 50% ethanol solution containing the fluorescent contrast agents acridine orange (40 µg/ml; #10050, Electron Microscopy Sciences) and sulforhodamine 101 (40 µg/ml; S7635, Sigma-Aldrich) for 2 minutes (Fig. 1A). Acridine orange stains DNA similar to hematoxylin, while sulforhodamine 101 stains cytosol and stroma similar to eosin³³. The specimens were then rinsed for 30 seconds in saline to remove excess dye and placed on a specimen holder with a glass window for imaging with a nonlinear microscope.

The nonlinear microscope²⁷ used a short-pulsed laser at 1030 nm wavelength to excite acridine orange and sulforhodamine 101 fluorescence in a narrow focus, providing visualization of a thin section without physical sectioning. The microscope had two interchangeable objectives: a 10x, 0.45 numerical aperture (CFI Plan Apo Lambda, Nikon) and a 5x, 0.25 numerical aperture objective (Fluar, Carl Zeiss). Fluorescent light from acridine orange and sulforhodamine 101 was detected using two photomultiplier tubes (H7422–40p, Hamamatsu). A white light camera was integrated into the nonlinear microscope to record a gross view of the specimen.

Specimens were evaluated on the nonlinear microscope in two modes: *real-time nonlinear microscopy mode* which emulates the procedure pathologists use with a standard microscope to evaluate histology and *auto-scan nonlinear microscopy mode* which emulates

a digital slide scanner. In real-time nonlinear microscopy mode, shown in Fig. 1B, pathologists examined the specimens on a computer monitor showing nonlinear microscopy images at 16 frames/second while translating the specimen to select the nonlinear microscopy field of view. Images resembling paraffin H&E were generated from nonlinear microscopy by displaying the fluorescence signals from the nuclear (acridine) and stromal (sulforhodamine) detector channels in an H&E color scale using an algorithm called Virtual Transillumination Microscopy.³⁴ A fiducial marker (shown in red in Fig. 1B) was displayed on the white-light gross image of the specimen indicating the current position of the nonlinear microscopy image to aid in navigation. The objectives could be rapidly changed for variable magnification and focus depth adjusted for visualizing tissue below the specimen surface. The real-time mode evaluation, including nonlinear microscopy images at known positions, was saved for post-procedural analysis and training. In this mode of operation, a pathologist can rapidly and efficiently evaluate large specimen areas, similar to slide evaluation on a standard histology microscope.

In auto-scan nonlinear microscopy mode (Fig. 1C), a nonlinear microscopy image of the entire specimen was generated by automatically acquiring a series of overlapping, high magnification 1×1 mm, 2048×2048 pixel frames with $1.2 \mu\text{m}$ lateral optical resolution²⁷ and $0.49 \mu\text{m}$ pixel size. The nonlinear microscopy frames were stitched together (using Microsoft Image Composite Editor) and viewed analogously to a whole slide image from a digital slide scanner. The auto-scan mode is more time-consuming than real-time mode and only acquires a limited number of image depths, however it enables multiple readers to evaluate nonlinear microscopy image data offline.

After evaluation with nonlinear microscopy, the fresh specimens were fixed in formalin on the glass surface of the specimen holder to avoid distortion of the imaged region by specimen handling, then processed for conventional paraffin H&E. The paraffin H&E slides were scanned with a digital slide scanner (20x magnification; Aperio AT2, Leica Biosystems Inc.).

Blinded Reading

Three pathologists (a senior pathologist with over 20 years of experience, a junior pathologist with less than 5 years of experience, and a pathology resident) evaluated nonlinear microscopy images and corresponding paraffin H&E in a prospective blinded reading consisting of training, pretesting, and reading phases. This protocol, outlined in Fig. 2, was used to assess the accuracy of detecting carcinoma on radical prostatectomy specimens using nonlinear microscopy. Intraoperative Gleason scoring of radical prostatectomies is typically not required and thus excluded in our analysis.

Training—The pathologists were trained in three steps. In the first step, pathologists evaluated fresh tissue in real-time nonlinear microscopy mode for at least 30 minutes to gain familiarity with nonlinear microscopy imaging and ergonomics. In the second step, pathologists reviewed 8 prerecorded real-time nonlinear microscopy evaluation procedure videos (Fig. 1B(ii)) (each ~5–10 mins in length) from 8 different patients. This step provided experience with various prostate pathologies visualized in fresh tissue on nonlinear

microscopy. In the final training step, the pathologists reviewed images from real-time imaging procedures that emphasized the differences and similarities between nonlinear microscopy and paraffin H&E. These differences and similarities were described previously.³² The nonlinear microscopy training was performed using real-time nonlinear microscopy mode due to the ease and rapidity of capturing large areas of varying pathologies. The training step took approximately 3 hours for each pathologist.

Pretesting and reading—122 freshly excised prostate specimens with an average size of 10 × 10 mm were collected from 40 patients and imaged in auto-scan nonlinear microscopy mode. Corresponding paraffin H&E slides were made and scanned on a slide scanner. The nonlinear microscope was operated in auto-scan nonlinear microscopy mode to enable evaluation of the same specimen area by multiple pathologists and enable high correspondence between the nonlinear microscopy imaging plane and the paraffin H&E slide. The nonlinear microscopy images and scanned paraffin H&E slides were viewed in OpenSeaDragon, a web-based viewer that enables variable magnification review. Nonlinear microscopy data from 6 specimens was discarded due to poor correspondence between the nonlinear microscopy and paraffin H&E image planes or because of poor tissue preservation unrelated to the study. These mismatches between the plane of nonlinear microscopy imaging and paraffin H&E slide occur because the nonlinear microscopy image is acquired on freshly excised tissue and the paraffin H&E slide requires tissue processing and microtome sectioning.

In pretesting, pathologists read 15 nonlinear microscopy images for the presence or absence of cancer. Corresponding paraffin H&E slides were then read to provide immediate feedback. After training and pretesting, the pathologists read nonlinear microscopy images of the remaining 101 specimens in a randomized order, blinded to paraffin H&E results, and recorded whether cancer was present or absent. After a washout period of one week, the pathologists read the paraffin H&E slides. A consensus diagnosis was obtained for paraffin H&E readings in the event of reader discrepancy in order to have a gold-standard diagnosis for comparison.

Statistical Analysis

The sensitivity, specificity, positive predictive value, negative predictive value, and accuracy of nonlinear microscopy assessment for the presence of cancer was calculated for each nonlinear microscopy reader using the consensus paraffin H&E diagnosis as the gold-standard. The 95% confidence intervals were calculated on the pooled results from the 3 readers. The interobserver variability was calculated using Fleiss kappa. A two-sample t test was used to compare the mean time required to evaluate the nonlinear microscopy images and paraffin H&E.

RESULTS

Nonlinear Microscopy Images of Fresh Prostate Specimens

Example nonlinear microscopy images of fresh prostate specimens are shown in Fig. 3 and 4. In these figures, differences between nonlinear microscopy images of fresh specimens and

paraffin H&E including cytoplasmic color difference, increased eosinophilic secretions in carcinoma, diminishment of cell border clarity, expanded cellular appearance, and images that appear thicker than paraffin H&E, are apparent, but these differences do not impair interpretation.³² Prostate carcinoma with poorly formed and fused glands (Gleason 4) is shown in Fig. 3A (nonlinear microscopy) and B (paraffin H&E). Figures 3C and 3D show an example of foamy gland adenocarcinoma visualized with nonlinear microscopy and paraffin H&E, respectively. The foamy appearance is not as apparent in the nonlinear microscopy image and instead the cytoplasm appears more eosinophilic. The bright intraluminal eosinophilic secretions seen in the nonlinear microscopy image commonly appear in fresh tissue visualization of carcinoma and is particularly evident in foamy gland variant. An example of mucinous fibroplasia visualized with nonlinear microscopy and paraffin H&E is shown in Fig. 3E and 3F. Collagenous micronodules are seen with associated eosinophilic stroma. Figures 4A and 4B show glomeruloid and cribriform patterns, respectively. Figure 4C is an example of perineural invasion. Figure 4D shows prominent nucleoli in a malignant gland, exemplifying the cytological detail present in nonlinear microscopy images of fresh tissue. In these example images, typical histological features of carcinoma (prominent nucleoli, glandular and stromal architectural patterns) are readily apparent in nonlinear microscopy and enable specimen reading and interpretation.

Sensitivity and Specificity

Table 1 summarizes the blinded reading results of the 101 specimens (61 with cancer present on paraffin H&E, 40 without cancer present). All three pathologists had a 95% or greater sensitivity and a 100% specificity. The pooled sensitivity was 97.3% (93.7%–99.1%; 95% confidence interval) and specificity was 100.0% (97%–100%). Interobserver agreement between the three pathologists was almost perfect for the nonlinear microscopy readings with a Fleiss $\kappa=0.95$. The three individual pathologists required an average of 39.2, 53.5, and 73.7 seconds to evaluate each nonlinear microscopy image and 38.6, 57.0, and 59.4 seconds to evaluate each paraffin H&E slide giving a combined average time of 55.4 seconds per nonlinear microscopy image and 51.7 seconds per paraffin H&E slide. These mean times were not statistically different in a two-sample t test ($p=0.76$).

DISCUSSION

In this study, we show that nonlinear microscopy with rapid fluorescent staining enables cancer detection with nearly equivalent accuracy (98%) to that of paraffin H&E with only a short training period. Specimen preparation requires <3 minutes after grossing, is non-destructive (no freezing or microtome sectioning), and enables gold-standard histological post-operative analysis of the same specimen. In this blinded reading, small fragments of tissue (10 × 10 mm) were used to represent localized detection of prostate cancer, however, multi-centimeter, fresh whole-mount specimens can also be evaluated on the nonlinear microscope without increasing specimen preparation times. Furthermore, several specimens can be prepared in parallel without additional specialized equipment because staining only requires a container for the fluorescent solution.

Because the nonlinear microscope can operate in real-time and auto-scan modes, it combines the analogous capabilities of traditional light microscopy and whole slide scanning in a single instrument. In both of these modes, the time to scan an area increases as the image resolution increases. In this study, we acquired data using auto-scan mode, which restricts imaging to a single objective for the entire specimen. Using this mode, we found that acquiring data using a 10x, 0.45 numerical aperture objective was sufficient for cancer detection in large specimens, while maintaining rapid data acquisition times. Real-time mode enables rapid surveying of large areas of tissue at user-specified magnifications and is thus the proposed mode for intraoperative evaluation of fresh tissue. Real-time mode was also used for pathologist training since the trainees could directly operate the microscope and observe a multitude of different specimens efficiently. This mode of operation, however, does not provide unbiased images of specimens because the operator controls the specimen translation, speed, and magnification, and therefore it is not appropriate for a blinded reading. Although the auto-scan mode is slower to acquire data, it enables evaluation of the same specimen by multiple different pathologists unbiased to the other's evaluation. Because it also enables specimen image archiving for offline viewing, the auto-scan mode was naturally conducive to this reading study.

There are several differences observed when evaluating fresh, unprocessed tissue with nonlinear microscopy. These differences include: variations in cytoplasmic color which is typically more basophilic in carcinoma on nonlinear microscopy than paraffin H&E; an increased frequency and volume of eosinophilic intraluminal secretions in carcinoma when visualized in fresh tissue with nonlinear microscopy than on processed tissue with paraffin H&E; loss of cell border sharpness and a thicker appearance of nonlinear microscopy images on fresh tissue due to the tissue not being dehydrated or processed with paraffin. These differences, however, are consistent and, combined with the ability to rapidly image multiple depths (analogous to serial sections), can augment interpretation of fresh tissue. Therefore, with training and experience, pathologists became accurate and comfortable interpreting these differences as evidenced by the high sensitivity and specificity (97.3% and 100%, respectively) and inter-observer agreement reported in this study.

Blinded reading of surgical margins with nonlinear microscopy was not practical in this study because positive margin rates are low and large numbers of specimens representing surgical margins were not available. However, we have previously demonstrated nonlinear microscopy imaging of extra-prostatic extension and positive surgical margins³² and typical histological features of carcinoma (prominent nucleoli, glandular and stromal architectural patterns) are independent of its location and were readily apparent in nonlinear microscopy images. Furthermore, this study used small fragments of tissue (average 10 × 10 mm) to assess localized cancer detection. Finally, diagnostic performance is expected to further improve when nonlinear microscopy is operated in real-time mode because the pathologist can adjust the instrument and view different depths continuously, while data from auto-scan nonlinear microscopy mode is limited to a few depth planes. This study provides evidence that nonlinear microscopy has a high diagnostic performance for assessing prostate cancer and may be a promising method for intraoperative specimen evaluation.

Gleason scoring would typically not be performed intraoperatively and therefore is not included in this study. Instead, we plan to analyze Gleason scoring accuracy in a separate study on needle core biopsies where it might be used clinically. Our initial studies, which include use of higher magnification objectives with smaller fields of view, suggest that Gleason scoring is feasible but requires increased reading time. There are challenges when interpreting Gleason patterns due to the differences in nonlinear microscopy image for fresh tissue versus paraffin H&E as described above, including thicker appearing sections, increased luminal secretions, and variation in simulated staining colors. However, nonlinear microscopy can generate images at adjustable depths up to 100 μm below the tissue surface, analogous to serial sectioning, which may enhance interpretation of Gleason patterns.

Many studies have investigated the utility of frozen sections in intraoperative evaluation of prostate margins.^{35–37} In order to avoid excessively prolonging surgical time, these studies have often restricted frozen sections to a small number of specimens representing a limited fraction of the margin or grossly suspicious areas and have reported wide variations in sensitivity for detecting positive margins.^{35–38} Recent studies using more comprehensive frozen section sampling of prostatectomy specimens demonstrated high sensitivities for detecting positive surgical margins, enabling an increase in the rate of nerve-sparing radical prostatectomies and a reduction in positive surgical margins.^{18,19,39,40} For example, in a study of over 11,000 patients, NeuroSAFE¹⁸ demonstrated a significant increase in nerve-sparing radical prostatectomy rates in (81% to 97% in all tumor stages) with a decrease in positive margins rates when using frozen sections. However, NeuroSAFE required processing up to 25 frozen sections per patient, with 5 cryostats, 2 pathologists, and 4 technicians to maintain a 35-minute average evaluation time. This and other studies demonstrated that intraoperative margin evaluation can improve nerve-sparing radical prostatectomy and positive surgical margin rates, but comprehensive sampling required extensive personnel, which is impractical and expensive for most hospitals and surgical workflows.^{18–20}

The present study suggests that nonlinear microscopy has sufficient accuracy for rapid evaluation of prostate tissue, achieving a pooled 97.3% sensitivity and 100% specificity for detecting carcinoma compared to paraffin H&E in a blinded reading by three pathologists. In contrast to frozen section analysis, nonlinear microscopy imaging does not require freezing and microtome sectioning. Multiple specimens can be prepared for imaging in parallel and large specimens can be imaged without requiring dissection into smaller sizes. Pathologists can begin nonlinear microscopy assessment within 3 minutes after inking and grossing. These advances can support future studies investigating comprehensive nonlinear microscopy evaluation of radical prostatectomy margins, comparable to the NeuroSAFE, with many fewer personnel and shorter evaluation times. Accurate, safe, and efficient intraoperative margin assessment could improve decisions regarding nerve-sparing without increasing positive margin rates.

Acknowledgments

We thank H. Ye and O. M. Carrasco-Zevallos for scientific support and preliminary data collection. This study was supported in part by the National Institutes of Health R01-CA178636-05, R01-CA075289-20, F32-CA183400-02, Air Force Office of Scientific Research (AFOSR) contracts FA9550-12-1-0551 and FA9550-15-1-0473, the MIT

Broshy Graduate Fellowship in Medical Engineering and Science, and Thorlabs. This work was conducted with support from Harvard Catalyst | The Harvard Clinical and Translational Science Center (National Center for Advancing Translational Sciences, National Institutes of Health Award UL 1TR002541) and financial contributions from Harvard University and its affiliated academic healthcare centers. The content is solely the responsibility of the authors and does not necessarily represent the official views of Harvard Catalyst, Harvard University and its affiliated academic healthcare centers, or the National Institutes of Health. MGG is currently in the Department of Biomedical Engineering, University of Rochester.

References

1. American Cancer Society. Cancer Facts & Figures 2018. 2018.
2. Bill-Axelson A, Holmberg L, Garmo H, Taari K, Busch C, Nordling S, et al. Radical Prostatectomy or Watchful Waiting in Prostate Cancer — 29-Year Follow-up. *N Engl J Med* 2018;379:2319–2329. [PubMed: 30575473]
3. Dell'Oglio P, Karnes RJ, Joniau S, Spahn M, Gontero P, Tosco L, et al. Very long-term survival patterns of young patients treated with radical prostatectomy for high-risk prostate cancer. *Urol Oncol Semin Orig Investig* 2016;34:234.e13–234.e19.
4. Hamilton ZA, Kane CJ. Nerve-sparing Technique During Radical Prostatectomy and its Effect on Urinary Continence. *Eur Urol* 2016;69:590–591. [PubMed: 26320380]
5. Michl U, Tennstedt P, Feldmeier L, Mandel P, Oh SJ, Ahyai S, et al. Nerve-sparing surgery technique, not the preservation of the neurovascular bundles, leads to improved long-term continence rates after radical prostatectomy. *Eur Urol* 2016;69:584–589. [PubMed: 26277303]
6. Bianco FJ, Scardino PT, Eastham JA. Radical prostatectomy: Long-term cancer control and recovery of sexual and urinary function (“trifecta”). *Urology* 2005;66:83–94. [PubMed: 16194712]
7. Sacco E, Prayer-Galetti T, Pinto F, Fracalanza S, Betto G, Pagano F, et al. Urinary incontinence after radical prostatectomy: incidence by definition, risk factors and temporal trend in a large series with a long-term follow-up. *BJU Int* 2006;97:1234–1241. [PubMed: 16686718]
8. Catalona WJ, Carvalhal GF, Mager DE, Smith DS. Potency, continence and complication rates in 1,870 consecutive radical retropubic prostatectomies. *J Urol* 1999;162:433–438. [PubMed: 10411052]
9. Sanda MG, Dunn RL, Michalski J, Sandler HM, Northouse L, Hembroff L, et al. Quality of Life and Satisfaction with Outcome among Prostate-Cancer Survivors. *N Engl J Med* 2008;358:1250–1261. [PubMed: 18354103]
10. Quinlan DM, Epstein JI, Carter BS, Walsh PC. Sexual Function following Radical Prostatectomy: Influence of Preservation of Neurovascular Bundles. *J Urol* 1991;145:998–1002. [PubMed: 2016818]
11. Rabbani F, Stapleton AMF, Kattan MW, Wheeler TM, Scardino PT. Factors predicting recovery of erections after radical prostatectomy. *J Urol* 2000;164:1929–1934. [PubMed: 11061884]
12. Kundu SD, Roehl KA, Eggener SE, Antenor JA V., Han M, Catalona WJ. Potency, continence and complications in 3,477 consecutive radical retropubic prostatectomies. *J Urol* 2004;172:2227–2231. [PubMed: 15538237]
13. Budäus L, Isbarn H, Schlomm T, Heinzer H, Haese A, Steuber T, et al. Current Technique of Open Intrafascial Nerve-Sparing Retropubic Prostatectomy. *Eur Urol* 2009;56:317–324. [PubMed: 19501454]
14. Ohori M, Kattan MiW, Koh H, Maru N, Slawin KM, Shariat S, et al. Predicting the Presence and Side of Extracapsular Extension: A Nomogram for Staging Prostate Cancer. *J Urol* 2004;171:1844–1849. [PubMed: 15076291]
15. Steuber T, Graefen M, Haese A, Erbersdobler A, Chun FK-H, Schlom T, et al. Validation of a Nomogram for Prediction of Side Specific Extracapsular Extension at Radical Prostatectomy. *J Urol* 2006;175:939–944. [PubMed: 16469587]
16. Partin AW, Kattan MW, Subong EN, Walsh PC, Wojno KJ, Oesterling JE, et al. Combination of prostate-specific antigen, clinical stage, and Gleason score to predict pathological stage of localized prostate cancer. A multi-institutional update. *JAMA* 1997;277:1445–1451. [PubMed: 9145716]

17. Augustin H, Eggert T, Wenske S, Karakiewicz PI, Palisaar J, Daghofer F, et al. Comparison of accuracy between the Partin tables of 1997 and 2001 to predict final pathological stage in clinically localized prostate cancer. *J Urol* 2004;171:177–181. [PubMed: 14665871]
18. Schlomm T, Tennstedt P, Huxhold C, Steuber T, Salomon G, Michl U, et al. Neurovascular Structure-adjacent Frozen-section Examination (NeuroSAFE) Increases Nerve-sparing Frequency and Reduces Positive Surgical Margins in Open and Robot-assisted Laparoscopic Radical Prostatectomy: Experience After 11 069 Consecutive Patients. *Eur Urol* 2012;62:333–340. [PubMed: 22591631]
19. von Bodman C, Brock M, Roghmann F, Byers A, Löppenberg B, Braun K, et al. Intraoperative Frozen Section of the Prostate Decreases Positive Margin Rate While Ensuring Nerve Sparing Procedure During Radical Prostatectomy. *J Urol* 2013;190:515–520. [PubMed: 23415965]
20. Vasdev N, Agarwal S, Rai BP, Soosainathan A, Shaw G, Chang S, et al. Intraoperative Frozen Section of the Prostate Reduces the Risk of Positive Margin Whilst Ensuring Nerve Sparing in Patients with Intermediate and High-Risk Prostate Cancer Undergoing Robotic Radical Prostatectomy: First Reported UK Series. *Curr Urol* 2016;9:93–103. [PubMed: 27390582]
21. Denk W, Strickler J, Webb W. Two-photon laser scanning fluorescence microscopy. *Science* 1990;248:73–76. [PubMed: 2321027]
22. Wang M, Kimbrell HZ, Sholl AB, Tulman DB, Elfer KN, Schlichenmeyer TC, et al. High-Resolution Rapid Diagnostic Imaging of Whole Prostate Biopsies Using Video-Rate Fluorescence Structured Illumination Microscopy. *Cancer Res* 2015;75:4032–4041. [PubMed: 26282168]
23. Wang M, Tulman DB, Sholl AB, Kimbrell HZ, Mandava SH, Elfer KN, et al. Gigapixel surface imaging of radical prostatectomy specimens for comprehensive detection of cancer-positive surgical margins using structured illumination microscopy. *Sci Rep* 2016;6:27419. [PubMed: 27257084]
24. Fereidouni F, Harmany ZT, Tian M, Todd A, Kintner JA, McPherson JD, et al. Microscopy with ultraviolet surface excitation for rapid slide-free histology. *Nat Biomed Eng* 2017;1:957–966.
25. Glaser AK, Reder NP, Chen Y, McCarty EF, Yin C, Wei L, et al. Light-sheet microscopy for slide-free non-destructive pathology of large clinical specimens. *Nat Biomed Eng* 2017;1:0084. [PubMed: 29750130]
26. Puliatti S, Bertoni L, Pirola GM, Azzoni P, Bevilacqua L, Eissa A, et al. Ex vivo fluorescence confocal microscopy: the first application for real-time pathological examination of prostatic tissue. *BJU Int* 2019;124:469–476. [PubMed: 30908852]
27. Giacomelli MG, Yoshitake T, Cahill LC, Vardeh H, Quintana LM, Faulkner-Jones BE, et al. Multiscale nonlinear microscopy and widefield white light imaging enables rapid histological imaging of surgical specimen margins. *Biomed Opt Express* 2018;9:2457. [PubMed: 29761001]
28. Cahill LC, Giacomelli MG, Yoshitake T, Vardeh H, Faulkner-Jones BE, Connolly JL, et al. Rapid virtual hematoxylin and eosin histology of breast tissue specimens using a compact fluorescence nonlinear microscope. *Lab Invest* 2018;98:150–160. [PubMed: 29131161]
29. Periasamy A, Skoglund P, Noakes C, Keller R. An Evaluation of Two-Photon Excitation Versus Confocal and Digital Deconvolution Fluorescence Microscopy Imaging in *Xenopus* Morphogenesis. 1999;181:172–181.
30. Helmchen F, Denk W. Deep tissue two-photon microscopy. *Nature* 2005;2:932–940.
31. Yoshitake T, Giacomelli MG, Quintana LM, Vardeh H, Cahill LC, Faulkner-Jones BE, et al. Rapid histopathological imaging of skin and breast cancer surgical specimens using immersion microscopy with ultraviolet surface excitation. *Sci Rep* 2018;8:4476. [PubMed: 29540700]
32. Cahill LC, Fujimoto JG, Giacomelli MG, Yoshitake T, Wu Y, Lin DI, et al. Comparing histologic evaluation of prostate tissue using nonlinear microscopy and paraffin H&E: a pilot study. *Mod Pathol* 2019;32:1158–1167. [PubMed: 30914763]
33. Robertson T, Bunel F, Roberts M. Fluorescein Derivatives in Intravital Fluorescence Imaging. *Cells* 2013;2:591–606. [PubMed: 24709799]
34. Giacomelli MG, Husvagt L, Vardeh H, Faulkner-Jones BE, Hornegger J, Connolly JL, et al. Virtual Hematoxylin and Eosin Transillumination Microscopy Using Epi-Fluorescence Imaging. *PLoS One* 2016;11:e0159337. [PubMed: 27500636]

35. Lepor H, Kaci L. Role of intraoperative biopsies during radical retropubic prostatectomy. *Urology* 2004;63:499–502. [PubMed: 15028445]
36. Gillitzer R, Thuroff C, Fandel T, Thomas C, Thuroff JW, Brenner W, et al. Intraoperative peripheral frozen sections do not significantly affect prognosis after nerve-sparing radical prostatectomy for prostate cancer. *BJU Int* 2011;107:755–759. [PubMed: 20880193]
37. Heinrich E, Schön G, Schiefelbein F, Michel MS, Trojan L. Clinical impact of intraoperative frozen sections during nerve-sparing radical prostatectomy. *World J Urol* 2010;28:709–713. [PubMed: 20358209]
38. Nunez AL, Giannico GA, Mukhtar F, Dailey V, El-Galley R, Hameed O. Frozen section evaluation of margins in radical prostatectomy specimens: A contemporary study and literature review. *Ann Diagn Pathol* 2016;24:11–18. [PubMed: 27649947]
39. Beyer B, Schlomm T, Tennstedt P, Boehm K, Adam M, Schiffmann J, et al. A feasible and time-efficient adaptation of NeuroSAFE for da Vinci robot-assisted radical prostatectomy. *Eur Urol* 2014;66:138–144. [PubMed: 24411279]
40. Preisser F, Theissen L, Wild P, Bartelt K, Kluth L, Köllermann J, et al. Implementation of Intraoperative Frozen Section During Radical Prostatectomy: Short-term Results from a German Tertiary-care Center. *Eur Urol Focus* 2019.

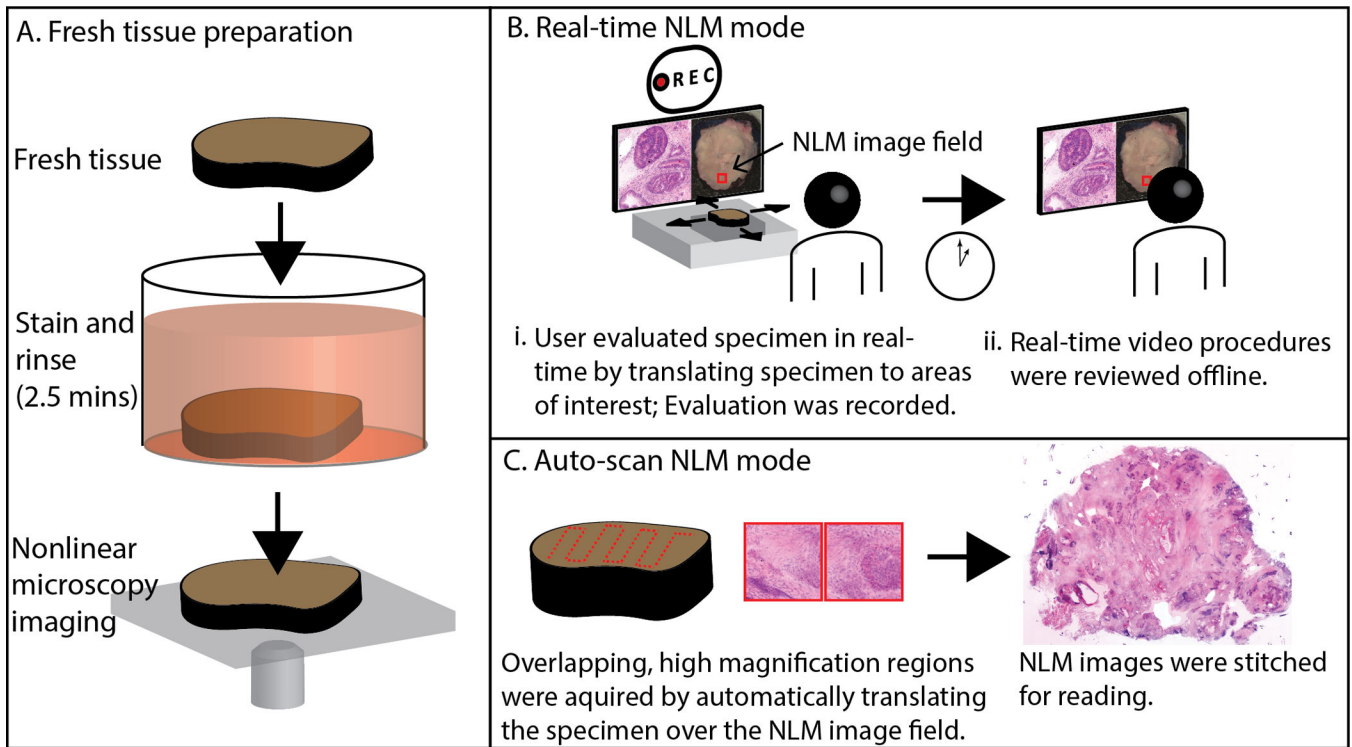


Fig. 1.

Method for evaluating fresh prostate tissue using nonlinear microscopy (NLM). **A.** Fresh tissue was stained in acridine orange and sulforhodamine 101 for 2 minutes, then rinsed in saline for 30 seconds. The specimen was placed on a glass specimen holder and transferred to the nonlinear microscope. The nonlinear microscope was operated in two modes: real-time nonlinear microscopy mode and auto-scan nonlinear microscopy mode. **B.** Real-time nonlinear microscopy mode: A white-light photograph of the specimen surface was displayed with a fiducial marker (in red) indicating the current nonlinear microscopy imaging field, providing a navigational guide. **B(i)** Pathologists examined the specimens on a computer monitor showing nonlinear microscopy images in an H&E color scale at 16 frames/second while translating the specimen to select the nonlinear microscopy field of view. The nonlinear microscopy evaluation procedure was recorded for offline, post-procedural review (**B(ii)**). **C.** Auto-scan nonlinear microscopy mode: a nonlinear microscopy image of the entire specimen cross section was generated by automatically acquiring a series of overlapping, high magnification regions and stitching them together.

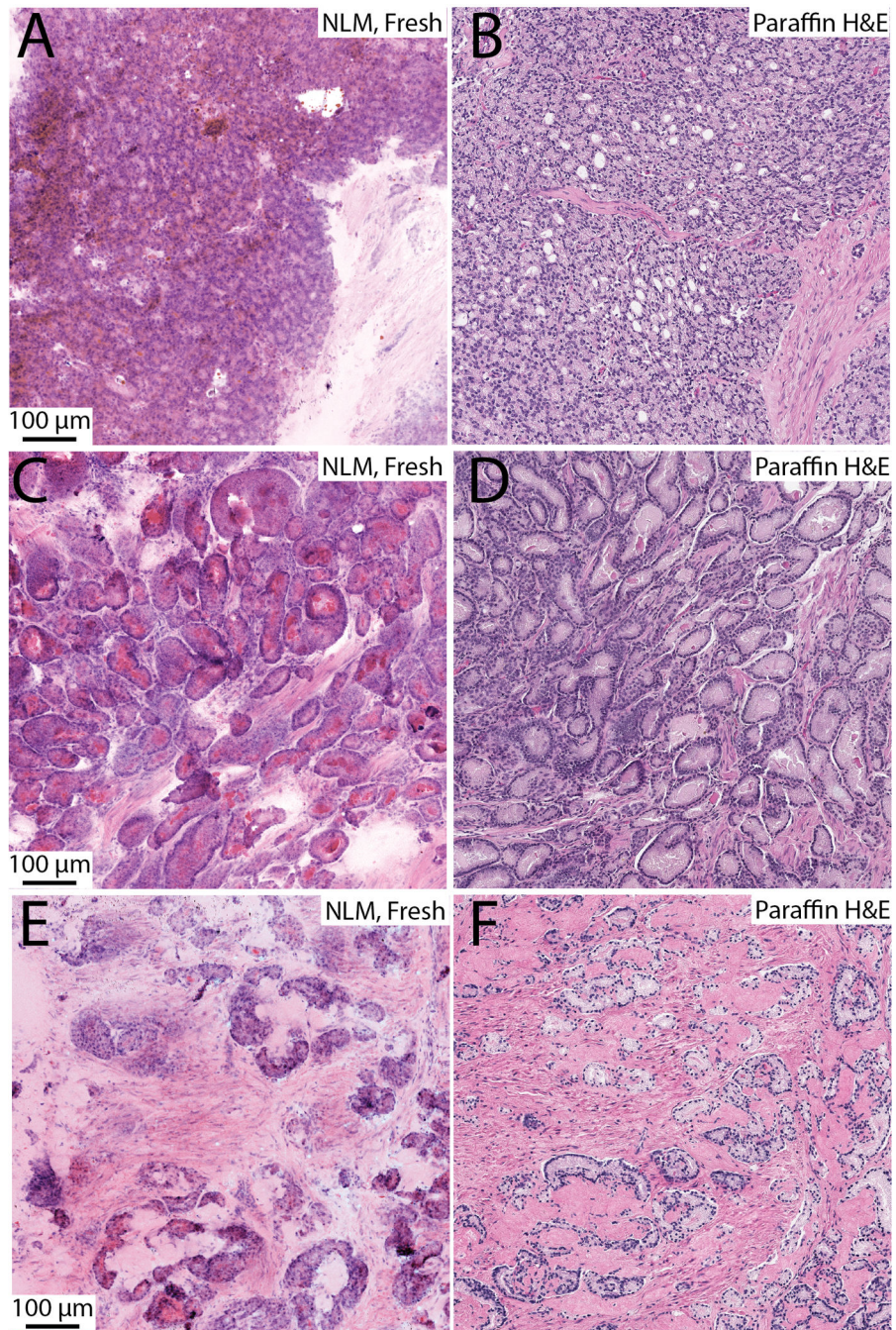


Fig. 3. Example nonlinear microscopy (NLM) images of fresh tissue pathology and corresponding paraffin H&E slides. **A, B.** Poorly formed and fused glands (Gleason 4); **C, D.** Foamy gland adenocarcinoma; **E, F.** Mucinous fibroplasia.

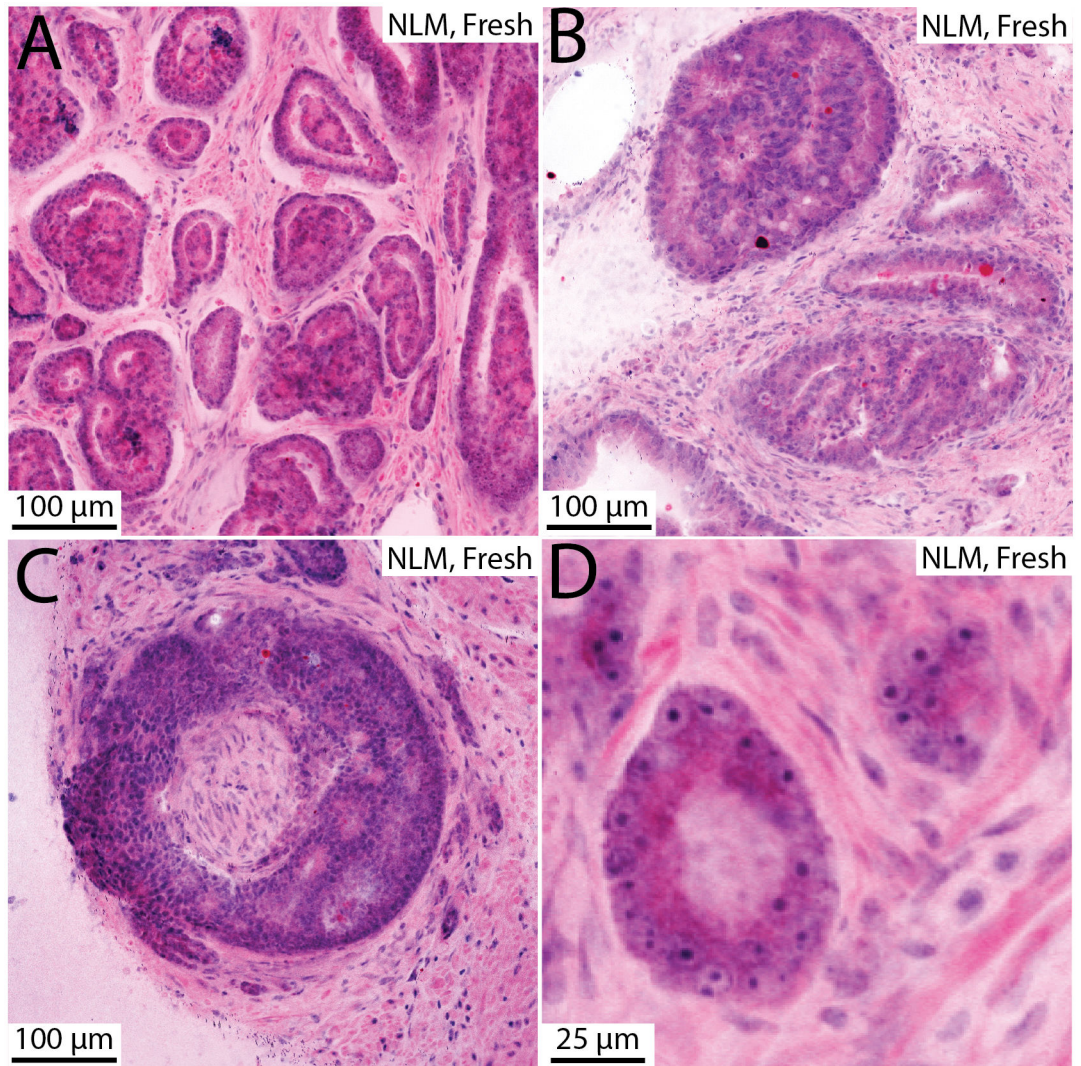


Fig. 4. Example nonlinear microscopy (NLM) images of carcinoma in fresh prostate tissue. **A.** Glomeruloid pattern. **B.** Cribriform. **C.** Perineural invasion. **D.** Large nucleoli visualized in malignant glands.

Table 1.

Sensitivity and specificity of nonlinear microscopy for detecting carcinoma in fresh prostate tissue vs paraffin H&E.

Reader	Sensitivity [95% CI]	Specificity [95% CI]	PPV	NPV	Accuracy
Reader 1	0.951	1.000	1.000	0.930	0.970
Reader 2	1.000	1.000	1.000	1.000	1.000
Reader 3	0.967	1.000	1.000	0.952	0.980
Pooled 1–3	0.973 [0.937, 0.991]	1.000 [0.970, 1.000]	1.000	0.960	0.983

Author Manuscript

Author Manuscript

Author Manuscript

Author Manuscript